

THE DETECTABILITY OF TRANSIT DEPTH VARIATIONS DUE TO EXOPLANETARY OBLATENESS AND SPIN PRECESSION

JOSHUA A. CARTER & JOSHUA N. WINN
 Kavli Institute for Astrophysics and Space Research,
 Massachusetts Institute of Technology, Cambridge, MA 02139
 carterja@mit.edu

Accepted for publication in The Astrophysical Journal

ABSTRACT

Knowledge of an exoplanet’s oblateness and obliquity would give clues about its formation and internal structure. In principle, a light curve of a transiting planet bears information about the planet’s shape, but previous work has shown that the oblateness-induced signal will be extremely difficult to detect. Here we investigate the potentially larger signals due to planetary spin precession. The most readily detectable effects are transit depth variations (T δ V) in a sequence of light curves. For a planet as oblate as Jupiter or Saturn, the transit depth will undergo fractional variations of order 1%. The most promising systems are those with orbital periods of approximately 15–30 days, which is short enough for the precession period to be less than about 40 years, and long enough to avoid spin-down due to tidal friction. The detectability of the T δ V signal would be enhanced by moons (which would decrease the precession period) or planetary rings (which would increase the amplitude). The *Kepler* mission should find several planets for which precession-induced T δ V signals will be detectable. Due to modeling degeneracies, *Kepler* photometry would yield only a lower bound on oblateness. The degeneracy could be lifted by observing the oblateness-induced asymmetry in at least one transit light curve, or by making assumptions about the planetary interior.

Subject headings: stars: planetary systems—techniques: photometric

1. INTRODUCTION

Measuring the oblateness of exoplanets would further our understanding of planetary formation, rotation, and internal structure. One possible measurement technique relies on the differences between the transit light curve of a spherical planet and an oblate planet with the same sky-projected area (Seager & Hui 2002, Barnes & Fortney 2003). However, the differences are minuscule, of order 200 parts per million (ppm) for a planet as oblate as Saturn, and 2 ppm for a “hot Jupiter” whose spin rate has been slowed by tidal friction into synchronization with its orbit. In a previous paper we showed that with this technique, even the best available light curves are only barely sufficient to rule out a Saturn-like oblateness (Carter & Winn 2009). Those results pertained to the planet HD 189733b, for which one would expect spin-orbit synchronization, and consequently the theoretical oblateness was an order of magnitude below the empirical upper limit.

In that work we also pointed out the potentially observable effects of a phenomenon that had been previously overlooked: the precession of the planet’s rotation axis. Precession of an oblate planet causes the sky-projected area of the planet to change over time, thereby causing gradual changes in the depth and duration of transits. In this paper we investigate the observable manifestations of spin precession in a broader context. Section 2 describes the characteristics of the signal in terms of the properties of the star, planet, and orbit. Section 3 discusses the range of orbital periods for which the signal is most readily detectable, considering the timescales for precession and spin-orbit synchronization. Section 4 presents simulated results for a specific case, a Saturn-like planet observed by the *Kepler* satellite. Section 5 summarizes and discusses the results.

2. CHARACTERISTICS OF THE SIGNAL

We model the planet as an oblate spheroid, illustrated in Figure (1). The *oblateness* (or *flatness*) parameter is defined as

$$f = \frac{R_{\text{eq}} - R_{\text{pol}}}{R_{\text{eq}}}, \quad (1)$$

where R_{eq} and R_{pol} are the equatorial and polar radii, respectively. For rotationally-induced oblateness, a good approximation is

$$f = \frac{3}{2}J_2 + \frac{1}{2} \frac{R_{\text{eq}}^3}{GM_p} \left(\frac{2\pi}{P_{\text{rot}}} \right)^2 \quad (2)$$

where M_p is the mass of the planet and J_2 is the planet’s zonal quadrupole moment (Murray & Dermott 2000, Hubbard 1984). This approximation is valid for all the Solar System planets for which f , J_2 and P_{rot} have been measured precisely.

The *obliquity* is the angle θ between the polar axis and the orbital axis. The angle ϕ specifies the direction of the projection of the polar axis onto the orbital plane. For a uniformly precessing planet, the case considered here, ϕ is a linear function of time,

$$\phi(t) = \frac{2\pi t}{P_{\text{prec}}} + \phi_0. \quad (3)$$

Accurate calculations of the transit light curve of an oblate spheroid, including the effects of stellar limb darkening, have been presented by Seager & Hui (2002), Barnes & Fortney (2003), and Carter & Winn (2009). In this paper we are not interested in high accuracy or in the slight differences between the light curve an oblate planet and a spherical planet. Instead we are interested in the order of magnitude of the variations in the transit depth and duration due to the changes in the precessing planet’s sky-projected figure.

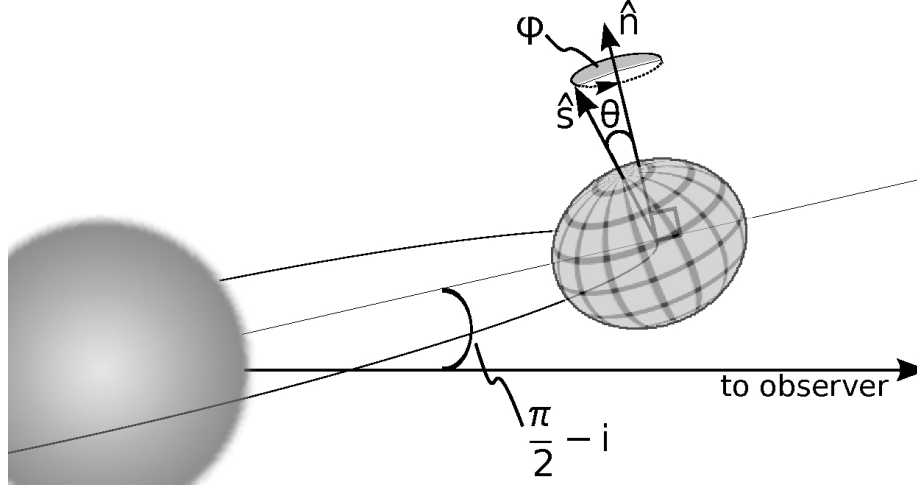


FIG. 1.— Geometry of transits by an oblate spheroid. The planet's orientation is specified by the spin-orbit obliquity $\theta \equiv \cos^{-1} \hat{s} \cdot \hat{n}$, the angle ϕ between the projection of the spin axis onto the orbital plane and the vector connecting the centers of the star and planet at midtransit, and the orbital inclination i relative to the sky plane.

In the absence of limb darkening, the depth δ is approximately the areal ratio between the sky projection of the oblate spheroid and the stellar disk,

$$\delta(t) = k^2 \sqrt{1 - \epsilon^2 \left\{ 1 - [\sin \theta \cos \phi(t) \sin i + \cos \theta \cos i]^2 \right\}} \quad (4)$$

where $k \equiv R_{\text{eq}}/R_*$ is the planet-to-star radius ratio, i is the orbital inclination with respect to the sky plane and ϵ is the ellipticity,

$$\epsilon \equiv \sqrt{1 - (1 - f)^2}. \quad (5)$$

A derivation of this expression is given in the Appendix. Figure 2 shows the fractional amplitude of the transit depth variations for the case $i = 90^\circ$, as a function of f and θ . For Saturn-like values of oblateness and obliquity, the depth variations would be a few percent.

The transit duration will also vary over the precession period, due to the changing dimension R_{\parallel} of the planet's sky projection in the direction of orbital motion:

$$R_{\parallel} = R_{\text{eq}} \sqrt{(1 - f_{\perp})^2 \sin^2 \theta_{\perp} + \cos^2 \theta_{\perp}}, \quad (6)$$

where

$$f_{\perp} \equiv 1 - \sqrt{1 - \epsilon^2 \left\{ 1 - [\sin \theta \cos \phi(t) \sin i + \cos \theta \cos i]^2 \right\}} \quad (7)$$

$$\theta_{\perp} \equiv \tan^{-1} \frac{\sin \phi(t) \tan \theta}{\cos \phi(t) \tan \theta \cos i - \sin i} \quad (8)$$

are the quantities describing the oblateness and obliquity of the projected exoplanet's shape. Derivations of these expressions are also given in the Appendix. For a circular orbit, the ingress/egress duration (first to second contact, or third to fourth contact) is approximately

$$\tau \approx \left(\frac{R_* P_{\text{orb}}}{\pi a} \right) \frac{R_{\parallel}}{R_*} \sqrt{1 - b^2}, \quad (9)$$

where P_{orb} is the orbital period, a is the orbital distance, and $b \equiv a \cos i / R_*$ is the normalized impact parameter. The full transit duration (first to fourth contact) is approximately (e.g.,

Seager & Mallén-Ornelas 2003)

$$T_{\text{full}} \approx \left(\frac{R_* P_{\text{orb}}}{\pi a} \right) \sqrt{\left[1 + \frac{R_{\parallel}}{R_*} \right]^2 - b^2}. \quad (10)$$

These approximations are valid as long as the transit is not too close to grazing. The fractional amplitude of the τ variations ($T\tau V$) is comparable to that of depth variations ($T\delta V$). The amplitude of transit full-duration variations (TDV) depends on k and b , in addition to f and θ , and therefore cannot be summarized in a single contour plot such as Figure 2.

3. THE OPTIMAL ORBITAL DISTANCE

In this section we suppose that the planet's precession is caused exclusively by the gravitational torque from the star. In order for the detection of precession-induced $T\delta V$ s or TDV s to be feasible, the planet must be close enough to the star for precession to produce observable effects in a human lifetime. However, if the planet is too close to the star, then tidal dissipation should slow down the planet's rotation until it is synchronized with the orbital period, and drive the obliquity to zero, which would cause the signal to be undetectable. Hence, we must ask if there is a range of distances from the star that is close enough for rapid precession, and yet far enough to avoid spin-orbit synchronization.

The spin precession period for a planet on a fixed circular orbit is given by

$$P_{\text{prec}} = \frac{13.3 \text{ yr}}{\cos \theta} \left(\frac{\mathbb{C}/J_2}{13.5} \right) \left(\frac{P_{\text{orb}}}{15 \text{ d}} \right)^2 \left(\frac{10 \text{ hr}}{P_{\text{rot}}} \right) \quad (11)$$

(Ward 1975), where P_{rot} is the planet's rotation period and \mathbb{C} is its moment of inertia divided by $M_p R_{\text{eq}}^2$. The numerical scaling of 13.5 for \mathbb{C}/J_2 is the estimated value for Saturn (Ward & Hamilton 2004). According to this expression, orbital periods shorter than $P_{\text{orb}} \sim 30$ days will lead to rapid enough precession to be observed over decadal timescales, depending on the planet's obliquity and internal structure. In Fig. 3, the thick solid line shows the spin precession period as a function of orbital distance, for an exoplanet with the same P_{rot} , \mathbb{C} , J_2 , and θ as Saturn. (The thin solid lines show the more rapid precession rates produced by hypothetical planetary satellites, as discussed in § 5.)

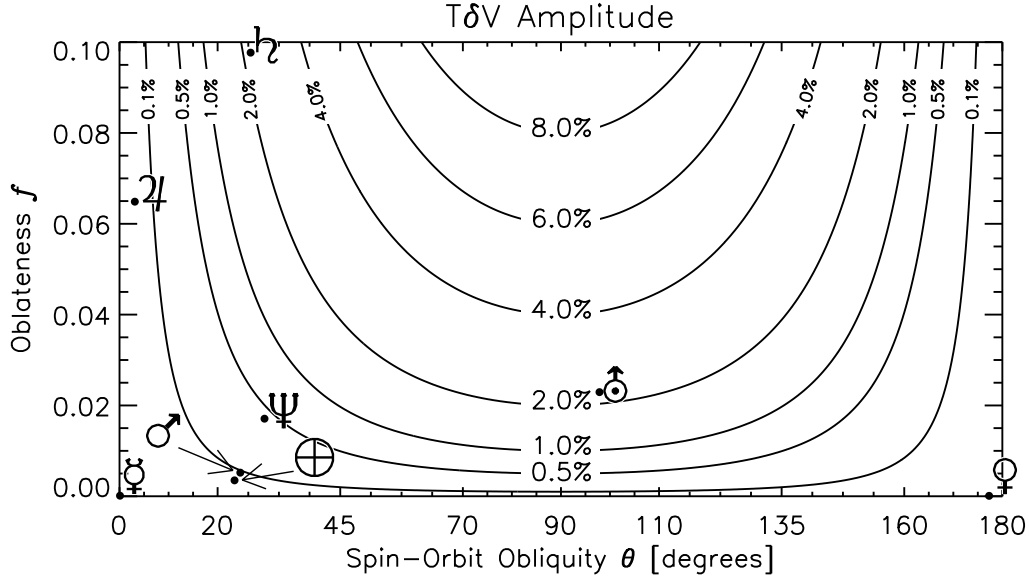


FIG. 2.— The fractional amplitude of transit depth variations (TδVs), shown as a function of oblateness (f) and obliquity (θ) assuming the orbit is perpendicular to the sky plane ($i = 90^\circ$). For reference, the astrological symbols show the shape parameters of Solar System planets: ☿ – Mercury, ♀ – Venus, ♁ – Earth, ♂ – Mars, ♃ – Jupiter, ♄ – Saturn, ♅ – Uranus, ♆ – Neptune.

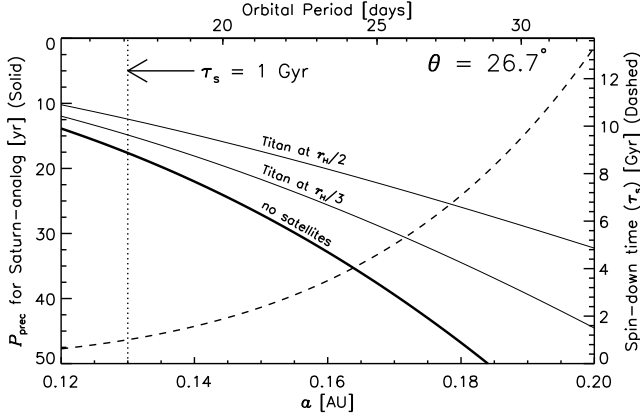


FIG. 3.— The optimal orbital distance. The solid curves refer to the axis on the left; they show the calculated spin precession period as a function of orbital distance for a Saturn-analog planet, with no satellites (thick line) and with a Titan-like satellite (thin lines) orbiting at a specified fraction of a Hill radius. The dashed curve refers to the axis on the right; it shows the calculated timescale for tidal spin-orbit synchronization. The vertical dotted line marks the orbital distance for which the spin-down time is 1 Gyr.

The approximate timescale for tidal spin-orbit synchronization is

$$\tau_s \approx 1.22 \text{ Gyr} \times \left(\frac{Q_p}{10^{6.5}} \right) \left(\frac{C}{0.25} \right) \left(\frac{5 \text{ hr}}{P_{\text{rot},i}} - \frac{10 \text{ hr}}{P_{\text{rot}}} \right) \times \left(\frac{M_p}{M_{\text{Jup}}} \right) \left(\frac{R_{\text{Jup}}}{R_{\text{eq}}} \right)^3 \left(\frac{P_{\text{orb}}}{15 \text{ d}} \right)^4 \quad (12)$$

(Goldreich & Soter 1966), where Q_p is the planet's tidal dissipation factor and $P_{\text{rot},i}$ is its initial rotation period, both of which are highly uncertain.

Based upon Solar System constraints, Q_p is thought to be in the range 10–500 for terrestrial planets, and $10^{4.5-6.5}$ for gas or ice giant planets (Goldreich & Soter 1966, Peale et al. 1980, Yoder 1995, Mardling & Lin 2004, Ogilvie & Lin 2004, Jackson et al. 2008), although the results are strongly

model-dependent and also dependent on the frequency of tidal oscillations. In setting the scale parameters in Eqn. (12) we adopted $Q_p = 10^{6.5}$, on the high end of current estimates, giving the longest (most favorable) synchronization timescale.

The primordial spin period might be expected to be near the rotational breakup limit, which is ≈ 3 hr for Jupiter (Murray & Dermott 2000), although the effects of planetary contraction and disk-planet interactions should also be considered. For Eqn. (12) we used a current rotation period of 10 hr (similar to Jupiter and Saturn) and an initial period of 5 hr.

For $\tau_s \gtrsim 1$ Gyr, it is reasonable to hope that the planet has not yet been tidally spun down. Thus, with reference to Eqns. (11) and (12), the “sweet spot” for observing the effects of spin precession on the transit parameters is at $P_{\text{orb}} \sim 15$ d, which is long enough to allow for rapid rotation, and short enough to allow for rapid precession.

Of course the identification of a single optimal period is a simplification. The existence and observability of TδVs and TDVs depends on the particular mass and radius of the planet under consideration and the observed age of the star, as well as the parameters relating to the planet's tidal dissipation, internal constitution, and initial spin period. The dashed line in Figure 3 shows the dependence of τ_s on orbital distance for the particular case of a Saturn analog. Table 1 gives some numerical results for precession periods and synchronization timescales for hypothetical close-in planets with properties similar to Solar System planets. If we require $P_{\text{prec}} < 40$ yr and $\tau_s > 1$ Gyr for observability, then from Table 1 we see that the signal is potentially observable for Jupiter and Saturn analogs. For analogs of Uranus and Neptune, we expect the signal to be unobservable unless the spin precession is made more rapid by the presence of large satellites (see § 5). For Earthlike planets the signal seems unlikely to be observable because of strong tidal dissipation.

4. A SPECIFIC EXAMPLE

In this section we examine the particular case of a hypothetical, ringless, moonless, Saturn-like transiting exoplanet ($f = 0.1$, $\theta = 27^\circ$) in a circular orbit around a Sun-like star

TABLE 1
RELEVANT TIMESCALES FOR THE OBSERVABILITY OF PLANETARY SPIN PRECESSION

Planet analog ^a	Adopted planetary parameters					for $\tau_s = 1$ Gyr		for $P_{\text{prec}} = 40$ yr		Observable Range in P_{orb} [d]
	P_{rot}^i [hr]	P_{rot} [hr]	Q_p	C	C/J_2	P_{prec} [yr]	P_{orb} [d]	P_{orb} [d]	τ_s [Gyr]	
Jupiter	5.0	10.0	$10^{6.5}$	0.26	15.4	13.7	14.3	24.3	8.5	14.3 – 24.3
Saturn	5.0	11.0	$10^{6.5}$	0.22	13.5	15.7	17.1	27.3	6.5	17.1 – 27.3
Uranus	8.0	17.0	$10^{6.5}$	0.22	67.0	45.3	16.3	15.3	0.78	None ^a
Neptune	8.0	16.0	$10^{6.5}$	0.23	68.0	43.8	15.3	14.7	0.83	None ^a
Earth	12.0	24.0	$10^{2.0}$	0.34	314	13,100	151	8.40	9.0×10^{-6}	None ^a

REFERENCES. — Murray & Dermott (2000), Hubbard (1984), Yoder (1995), Ward & Hamilton (2004)

^a Assuming no satellites

with $P_{\text{orb}} = 17$ d. This orbit is near the “sweet spot,” giving $P_{\text{prec}} = 17$ yr and $\tau_s = 1$ Gyr.

4.1. Likelihood of discovery

First we must ask how likely it is that such a planet will be discovered. Giant planets with periods between 15–30 d are already known to exist from Doppler surveys. At the time of writing, the `exoplanets.org` database has 8 such planets. Indeed one of them is already known to transit (HD 17156b; Fischer et al. 2007), although in that case tidal effects may have slowed the planet’s rotation because the orbit is highly eccentric and the pericenter distance is small. None of the other 7 planets is known to transit, and the probability that at least one of them transits is approximately 23%. Given these facts and the recent acceleration in the discovery rate using the Doppler method, it would seem likely that a transiting gas giant with $P_{\text{orb}} = 15$ –30 d will be discovered in the near future.

Of particular interest are the prospects for the *Kepler* satellite mission (Borucki et al. 2010). *Kepler* searches for transiting planets by keeping $\approx 10^5$ stars under nearly continuous photometric surveillance for at least 3.5 yr and possibly as long as 6 yr. To estimate the fraction of the target stars that has a suitable planet, we used the power-law formulas given by Cumming et al. (2008) for the abundance of planets of a given mass and period, which were derived from data from the Keck Planet Search. The integrated value of (abundance \times transit probability) over the range $P_{\text{orb}} = 15$ –30 d, $M_p = 0.2$ –2 M_{Jup} is approximately 0.019%. Therefore, among the 5×10^4 Sun-like stars in the *Kepler* field, we expect ≈ 10 transiting giant planets with $P_{\text{orb}} = 15$ –30 d.

4.2. Expected signal

Figure 4 shows the expected time variations in δ , τ , and T_{full} for our hypothetical close-in Saturn. Compared to the T δ V signal, the TDV signal has a smaller amplitude, and depends on a larger number of parameters. The T τ V signal has a similar amplitude to the T δ V signal, but τ cannot be measured as precisely as δ because of the relatively short duration of the partial transit phases. Therefore we expect the T δ V signal to provide the best constraints on the planetary shape parameters.

Depth variations of a few percent should be detectable. Ground-based observations of individual transits have already allowed δ to be measured to within 1% [see, e.g., Gillon et al. (2009), Johnson et al. (2009), Winn et al. (2009)]. To estimate the precision with which *Kepler* can measure transit depth variations, we simulated a transit light curve and averaged it into 30 min bins, corresponding to *Kepler*’s standard time sampling. Then we added white noise with a standard deviation of 95 ppm, as appropriate for a typical *Kepler* tar-

get (KIC r mag = 13), based on the early results of Welsh et al. (2010) and Latham et al. (2010). By fitting a parameterized model to the light curve we found that the transit depth was recovered to within 0.6%. Over a 6 yr mission, *Kepler* would observe ≈ 130 transits with this precision.

4.3. Parameters and degeneracies

Next we discuss the “inverse problem” of inferring the planetary shape and precession parameters from the observed T δ V signal. For $i = 90^\circ$, the T δ V signal is periodic with period $P_{\text{prec}}/2$. For $i \neq 90^\circ$ the T δ V period is actually P_{prec} , but the odd and even maxima have only slightly different amplitudes. Hence the period of the T δ V signal will reveal P_{prec} .

Three other characteristics of the T δ V signal will help to pin down the model parameters. First, the minimum observed transit depth will reveal the parameter combination

$$\delta_{\min} = k^2(1 - f) = k^2\sqrt{1 - \epsilon^2}. \quad (13)$$

Second, the full range of transit depths determines a combination of f and θ ,

$$\begin{aligned} \left[\frac{\delta_{\max}}{\delta_{\min}} \right]^2 - 1 &= \frac{\epsilon^2}{1 - \epsilon^2} (\sin i \sin \theta + \cos i \cos \theta)^2 \\ &= \frac{\epsilon^2}{1 - \epsilon^2} (\sin^2 \theta + \Delta i \sin 2\theta) + O(\Delta i)^2 \\ &\approx 2f \sin^2 \theta, \end{aligned} \quad (14)$$

where $\Delta i = \pi/2 - i$ is always small and can be measured precisely through transit photometry. Third, the phases at which the maxima occur will determine ϕ_0 .

For $\Delta i \neq 0$ there are two other informative observables, at least in principle. First, the phases at which the minima occur depends slightly on Δi and θ :

$$\phi_{\min} - \phi_0 = (2n - 1) \frac{\pi}{2} + \begin{cases} +\Delta i \cot \theta, & n \text{ odd} \\ -\Delta i \cot \theta, & n \text{ even} \end{cases} + O(\Delta i)^3, \quad (15)$$

where $n = 1, 2, 3, \dots$. Second, there is a slight difference in heights between odd and even maxima,

$$\Delta \delta_{\max} = \Delta i \frac{k^2 \epsilon^2 \sin 2\theta}{\sqrt{1 - \epsilon^2 \cos^2 \theta}} + O(\Delta i)^3, \quad (16)$$

but these effects are very small in practice. For our Saturn analog, assuming $i = 88.97^\circ$ (transit impact parameter = 0.5), the difference in the maxima is smaller than 0.25%.

For $\Delta i \neq 0$ there are a total of 6 observables listed above, and it would be possible in principle (with arbitrarily precise data) to determine all 6 model parameters k , f , θ , i , P_{prec} and ϕ_0 . However, using our simulated *Kepler* light curve we find

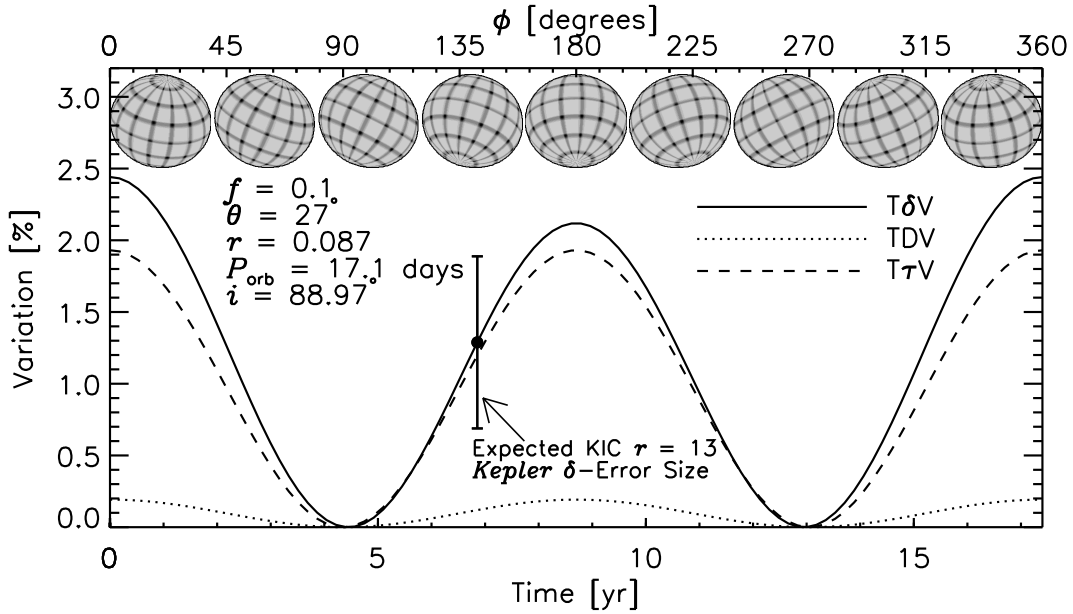


FIG. 4.— Variations in the transit light curve due to an oblate, oblique, precessing exoplanet. Plotted are the transit depth (δ), total duration (T_{full}) and ingress duration (τ) fractional variations (T δ V, TDV, and T τ V, respectively) that are expected for a uniformly precessing Saturn-like planet around a Sun-like star. The time scale is based on the assumption $P_{\text{orb}} = 17.1$ days.

that f and θ cannot be determined independently, although Eqn. (14) could be used to place a lower bound on f . The degeneracy is illustrated in Fig. (5).

To break the parameter degeneracy, one possibility is to arrange for high-cadence, high-precision observations of at least one transit, seeking the slight oblateness-induced anomalies that were described by Seager & Hui (2002) and Barnes & Fortney (2003). Observations of a single light curve would lead to constraints on the sky-projected oblateness and obliquity [see Eqns. (7) and (8)], which, together with the T δ V signal, would uniquely determine f and θ . The best time to schedule such observations would be near a minimum of the T δ V curve, when the light curve anomalies are largest.

This would be a challenging task, as the amplitude of the differences between the actual light curve and the best-fitting model of the transit of a spherical planet would be $\lesssim 100$ ppm. For this specific example, even *Kepler* photometry (with 1 min cadence) would be insufficient to detect the anomalies in a single transit. By observing 10 transits near the minimum of the T δ V signal (during which time the sky-projected quantities are constant to within 1%), *Kepler* could detect the signatures of oblateness and obliquity at the 1σ level, but the resulting constraints would be weaker than the constraints determined by an analysis of the T δ V signal. A significantly larger planet, or brighter host star, would be required for meaningful constraints.

Another possibility is to enforce additional physically-motivated relationships between parameters. In particular, we have already shown that the precession period is a function of k , f , θ , \mathbb{C} and J_2 [by combining Eqn. (2) with Eqn. (11)]. A further condition can be imposed on f , \mathbb{C} and J_2 , such as the Darwin-Radau approximation for planets in hydrostatic equilibrium (Murray & Dermott 2000):

$$\frac{J_2}{f} = -\frac{3}{10} + \frac{5}{2}\mathbb{C} - \frac{15}{8}\mathbb{C}^2. \quad (17)$$

Following this path, there are 8 model parameters (k , f , θ , i , P_{prec} , ϕ_0 , \mathbb{C} , J_2) with 2 physically-motivated constraints

among them. However there are only 5 quantities that are well determined from the photometric data [P_{prec} , ϕ_0 , $f \sin^2 \theta$, $k^2(1-f)$, i], leaving us still short by one observable or constraint from being able to determine all the parameters. For example, if one were willing to assume $\mathbb{C} = 0.23$, then we find from our simulated *Kepler* data that f , θ , J_2 and P_{prec} can be recovered with a precision of about 10%, and k is recovered within 1%.

Assigning \mathbb{C} a specific value is unrealistic, but for realistic planets one expects \mathbb{C} to be smaller than 0.4 (Murray & Dermott 2000). We repeated the analysis of our hypothetical T δ V signal, allowing \mathbb{C} to be a free parameter restricted to that range, with a uniform prior.¹ In effect we averaged the results over a range of \mathbb{C} deemed to be physically plausible. As might be expected, a strong degeneracy was observed between f and θ , as seen in Fig. (5). However, we were still able to determine J_2 to within 10%, and k to within 2%.

5. DISCUSSION

In this paper we have investigated the observability of changes to transit light curves resulting from the spin precession of an oblate, oblique exoplanet. The most readily detectable signal is the T δ V signal, the variation in transit depth due to the changing area of the planetary silhouette. The planets that seem most likely to exhibit detectable effects are those with periods between 15–30 days (around Sun-like stars), which is short enough for precession periods to be 40 yr or less, and long enough to hope that tidal spin-orbit synchronization has not taken place.

It is also important to consider other physical processes that could give rise to T δ V signals, and which might confound the interpretation of the data. Starspots and other types of stellar variability can produce transit depth variations. These can be recognized and taken into account by monitoring the star outside of transits, as is done automatically by the *Kepler*

¹ We also required $J_2 > 0$, which corresponds to $\mathbb{C} > 0.133$ according to the Darwin-Radau relation (Eqn. 17).

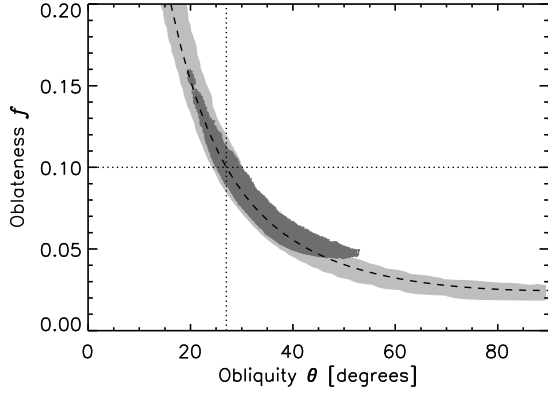


FIG. 5.— Hypothetical constraints on f and θ , as determined by analyzing a simulated TdV signal measured by *Kepler*. The signal was based on transits of a Saturn analog on a 17.1-day orbit around a Sun-like star with KIC $r = 13$ mag. The light gray region marks the 95% confidence region, using a model that allow the parameters $\{k, f, \theta, i, P_{\text{prec}}, \phi_0\}$ to be independent free parameters. In this case only the product $f \sin^2 \theta$ is well determined; the dashed line satisfies $f \sin^2 \theta = \text{constant}$. The dark gray region is the 95% confidence region, using a model that enforces the expected physical relationship between TdV amplitude and period, as well as the Darwin-Radau relation and a restricted range for the normalized moment of inertia \mathbb{C} . See § 4 for details. The dotted lines mark the “true” values of f and θ that were used to generate the simulated TdV signal.

satellite. We are not aware of any atmospheric phenomena associated with the exoplanet that would result in variations in the projected area at the 1% level, mimicking those due to uniform spin precession.

However, we can think of two plausible phenomena that would affect the TdV signal: moons and rings. If the planet has any moons then the precession period may be shorter than we have calculated. Satellites provide more leverage for the star to torque the exoplanetary system. Mathematically, satellites augment the effective values of J_2 and \mathbb{C} . Following Ward & Hamilton (2004) we may write the enhanced values as $J_2 + j$ and $\mathbb{C} + c$, where

$$c = \sum_i \frac{m_i}{M_p} \left(\frac{a_i}{R_{\text{eq}}} \right)^2 \frac{P_{\text{rot}}}{P_{\text{orb}}^i} \quad \text{and} \quad (18)$$

$$j = \frac{1}{2} \sum_i \frac{m_i}{M_p} \left(\frac{a_i}{R_{\text{eq}}} \right)^2 \frac{\sin(\theta - I_i)}{\sin \theta} \quad (19)$$

where m_i , a_i , I_i and P_{orb}^i are the satellites’ masses, orbital radii, orbital inclinations (relative to the planetary equator), and orbital periods.

For example, in the Saturnian system $j/J_2 \approx 3.2$ while $c/\mathbb{C} \approx 0.01$ such that $(\mathbb{C} + c)/(J_2 + j) \approx 3.2$ (as compared to $\mathbb{C}/J_2 = 13.5$). Titan alone is responsible for about 90% of j and c , shortening Saturn’s precession period by a factor of four relative to a satellite-free Saturn.² Fig. (3) shows the effect of Titan analogs at various distances around the Saturn analog considered in this paper. The distances are expressed

as fractions of the Hill radius r_H . This effect might be used to implicate the presence of exomoons, if a TdV signal were observed and found to correspond to an effective J_2 too large to be plausibly attributed to the planet alone.

Ring systems would increase the amplitude of the signal,

² For Titan: $a_i/R_{\text{eq}} = 20.2$, $m_i/M_p = 2.3 \times 10^{-4}$, $P_{\text{orb}}^i/P_{\text{rot}} = 38.3$; Murray & Dermott (2000).

while leaving the period unchanged. Optically thick rings that lie within the equatorial plane of the planet would increase the fractional variation of the sky-projected area, as the planet precesses. In contrast to exomoons, ring systems have little mass, and would not significantly reduce the precessional period. This is the situation in the Saturnian system (Ward & Hamilton 2004). It is not certain that rings could exist around planets having orbital periods between 15 and 30 days. Rings around planets with orbital periods less than $P_{\text{orb}} \approx 15$ days would likely be short-lived as a result of Poynting-Roberston drag amongst other destructive effects (Barnes & Fortney 2004). Also, we would be unlikely to find rings composed of water ice (e.g. Saturn’s rings) around planets whose orbits are interior to the snow line (< 1 AU). Nevertheless, rings of other compositions may exist.

In short, rings and moons would each affect the observed TdV signal, and in complementary ways. This may introduce some ambiguity in the estimation of the shape parameters of the rotating planet, but may also allow the rings and moons to be detectable, issues that we leave for future work.

For simplicity we have considered only circular orbits. Planets on eccentric orbits will undergo apsidal precession and nodal precession, which will result in time variable stellar torques on the planet and consequent modifications to the spin-axis precession. For Saturn or Jupiter analogs at $P_{\text{orb}} \gtrsim 15$ days, the apsidal and nodal precession periods are $\gtrsim 10^7$ yr and therefore likely to be irrelevant (Ragozzine & Wolf 2009).

In addition, we restricted our attention to the simplest case of uniform spin precession, but in reality the perturbations from other bodies may cause the spin axis to perform a more complex ballet. For example, Mars’s spin axis tumbles chaotically (Touma & Wisdom 1992). Saturn’s moon Titan causes a 700 yr modulation of Saturn’s spin precession frequency, due to its inclined orbit. Furthermore, Saturn’s spin axis may be trapped in a resonance with Neptune’s orbit, causing it to librate with an angular amplitude of $\gtrsim 31^\circ$ as it circulates about the second Cassini state (Ward & Hamilton 2004). These effects would be manifested as additional time dependences (“noise”) in the TdV signal. The effects are impossible to forecast for exoplanets, depending as they do on the existence of other bodies and any resonances that may occur.

We thank Dan Fabrycky, Darin Ragozzine, and members of the MIT exoplanet discussion group, for helpful conversations. We also thank an anonymous referee for helpful comments on an earlier draft of this manuscript.

APPENDIX

THE PROJECTION OF A SPHEROIDAL PLANET ONTO THE PLANE OF THE SKY

We model the planet as an oblate spheroid, illustrated in Figure (1). The sky plane projected shadow of the spheroidal planet is bounded by an ellipse. The polar axis, \hat{s} , of the spheroid is tilted by the obliquity angle $\theta > 0$ from the orbital axis \hat{n} and by the angle $\theta' > 0$ from the axis \hat{n}' which is perpendicular to the plane that is perpendicular to the sky plane. Let \hat{y} be the axis which lies along the line connecting the center of mass and the observer. Let \hat{x} be the axis in the orbital plane whose projection into the

plane perpendicular to the sky plane lies along \hat{y} . The angle ϕ is the angle through which \hat{s} is rotated about \hat{n} and ϕ' is the angle through which \hat{s} is rotated about \hat{n}' such that $\phi = \phi' = 0$ corresponds to the orientation in which the spheroid is tipped towards the observer (such that \hat{s} is coplanar with both \hat{x} and \hat{y}). It follows that

$$\cos \theta = \hat{s} \cdot \hat{n} \quad (\text{A1})$$

$$\cos \theta' = \hat{s} \cdot \hat{n}' \quad (\text{A2})$$

$$\cos \phi \sin \theta = \hat{s} \cdot \hat{x} \quad (\text{A3})$$

$$\cos \phi' \sin \theta' = \hat{s} \cdot \hat{y} \quad (\text{A4})$$

$$\hat{x} - \hat{y} = \hat{n} \cos i - \hat{x} (1 - \sin i) \quad (\text{A5})$$

where $i \equiv \sin^{-1} \hat{x} \cdot \hat{y}$ is the inclination of the orbital plane to the sky plane and where we have assumed the distance from planet to star is much less than the distance from planet to observer. The following relationship between unprimed angles (measured relative to the orbital plane) and primed angles (measured relative to the sky plane) may be derived from the above equations:

$$\cos \phi' \sin \theta' = \sin i \cos \phi \sin \theta + \cos i \cos \theta. \quad (\text{A6})$$

The polar axis of the spheroid is inclined relative to the plane of the sky by the angle θ'' where

$$\cos^2 \theta'' = 1 - \cos^2 \phi' \sin^2 \theta' \quad (\text{A7})$$

$$= 1 - (\sin i \cos \phi \sin \theta + \cos i \cos \theta)^2 \quad (\text{A8})$$

If \hat{p} and \hat{q} are the orthonormal axes in the sky plane that are aligned with the axes of the ellipse bounding the planet's shadow, then a point (y, p, q) on the surface of the spheroid satisfies

$$(y')^2 + p^2 + \left(\frac{q'}{1-f} \right)^2 = R_{\text{eq}}^2 \quad (\text{A9})$$

where

$$\begin{aligned} y' &= y \cos \theta'' - q \sin \theta'' \\ q' &= y \sin \theta'' + q \cos \theta'', \end{aligned}$$

R_{eq} is the equatorial radius and f is the oblateness parameter.

The analytic description of the closed curve bounding the projection of the planet on the sky plane may be found by solving for the non-degenerate solutions of $y(p, q)$ in Eqn. (A9). Non-degenerate solutions correspond to points in the sky plane where rays parallel with \hat{y} intersect at exactly one point on the planetary surface and thus define the boundary of the shadow as seen by the observer (who is located at a distant point along \hat{y}). As advertised, it may be shown that the collection of these points satisfy the equation of an ellipse,

$$p^2 + \frac{q^2}{\sin^2 \theta'' + (1-f)^2 \cos^2 \theta''} = R_{\text{eq}}^2, \quad (\text{A10})$$

having major and minor axis lengths, A and B , satisfying

$$A = R_{\text{eq}} \quad (\text{A11})$$

$$\begin{aligned} B &= R_{\text{eq}} \sqrt{\sin^2 \theta'' + (1-f)^2 \cos^2 \theta''} \\ &= R_{\text{eq}} \sqrt{1 - \epsilon^2 \cos^2 \theta''} \\ &= R_{\text{eq}} \sqrt{1 - \epsilon^2 \left[1 - (\sin i \cos \phi \sin \theta + \cos i \cos \theta)^2 \right]} \end{aligned} \quad (\text{A12})$$

where $\epsilon \equiv \sqrt{1 - (1-f)^2}$.

The minor axis of the ellipse lies along the projection of the polar axis onto the sky plane. The angle between the major axis of the ellipse and the direction of orbital motion is given as

$$\theta_{\perp} = \tan^{-1} \frac{\sin \phi \tan \theta}{\cos \phi \tan \theta \cos i - \sin i} \quad (\text{A13})$$

and the oblateness parameter of the ellipse, $f_{\perp} \equiv (A - B)/A$, is given as

$$f_{\perp} = 1 - \sqrt{1 - \epsilon^2 \left\{ 1 - [\sin \theta \cos \phi \sin i + \cos \theta \cos i]^2 \right\}}. \quad (\text{A14})$$

The boundary of the ellipse may be defined relative to the ellipse center via the parameter equations

$$X(s) = R_{\text{eq}} [\cos s \cos \theta_{\perp} - (1 - f_{\perp}) \sin s \sin \theta_{\perp}] \quad (\text{A15})$$

$$Y(s) = R_{\text{eq}} [\cos s \sin \theta_{\perp} + (1 - f_{\perp}) \sin s \cos \theta_{\perp}] \quad (\text{A16})$$

for $s \in [0, 2\pi]$ and where X is the coordinate along the direction of orbital motion. The radius, R_{\parallel} , of the projection of the ellipse onto the direction of orbital motion is equal to the maximum of $X(s)$. This maximum occurs for s_{\max} satisfying

$$\tan s_{\max} = -(1 - f_{\perp}) \tan \theta_{\perp} \quad (\text{A17})$$

for which

$$R_{\parallel} \equiv X(s_{\max}) = R_{\text{eq}} \sqrt{(1 - f_{\perp})^2 \sin^2 \theta_{\perp} + \cos^2 \theta_{\perp}}. \quad (\text{A18})$$

The areal ratio of the spheroidal planet's sky projection and the stellar disk is

$$\begin{aligned} \delta &= \frac{\pi AB}{\pi R_{\star}^2} \\ &= k^2 \sqrt{1 - \epsilon^2 \left[1 - (\sin i \cos \phi \sin \theta + \cos i \cos \theta)^2 \right]}. \end{aligned} \quad (\text{A19})$$

where $k \equiv R_{\text{eq}}/R_{\star}$.

REFERENCES

- Barnes, J. W., & Fortney, J. J. 2003, *ApJ*, 588, 545
 Barnes, J. W., & Fortney, J. J. 2004, *ApJ*, 616, 1193
 Carter, J. A., & Winn, J. N. 2010, *ApJ*, 709, 1219
 Cumming, A., Butler, R. P., Marcy, G. W., Vogt, S. S., Wright, J. T., & Fischer, D. A. 2008, *PASP*, 120, 531
 Goldreich, P., & Soter, S. 1966, *Icarus*, 5, 375
 Hubbard, W. B. 1984, *Planetary Interiors*, New York, Van Nostrand Reinhold Co., 1984, 343 p.,
 Jackson, B., Greenberg, R., & Barnes, R. 2008, *ApJ*, 678, 1396
 Latham, D. W., et al. 2010, *arXiv:1001.0190*
 Mardling, R. A., & Lin, D. N. C. 2004, *ApJ*, 614, 955
 Murray, C. D., & Dermott, S. F. 2000, *Solar System Dynamics*, by C.D. Murray and S.F. Dermott. Cambridge, UK: Cambridge University Press, 2000.,
 Ogilvie, G. I., & Lin, D. N. C. 2004, *ApJ*, 610, 477
 Peale, S. J., Cassen, P., & Reynolds, R. T. 1980, *Icarus*, 43, 65
 Ragozzine, D., & Wolf, A. S. 2009, *ApJ*, 698, 1778
 Seager, S., & Hui, L. 2002, *ApJ*, 574, 1004
 Seager, S., & Mallén-Ornelas, G. 2003, *ApJ*, 585, 1038
 Tوما, J., & Wisdom, J. 1993, *Science*, 259, 1294
 Ward, W. R. 1975, *Science*, 189, 377
 Ward, W. R., & Hamilton, D. P. 2004, *AJ*, 128, 2501
 Welsh, W. F., Orosz, J. A., Seager, S., Fortney, J. J., Jenkins, J., Rowe, J. F., Koch, D., & Borucki, W. J. 2010, *arXiv:1001.0413*
 Yoder, C. F. 1995, *Icarus*, 117, 250